Doppler-free Saturated Absorption Spectroscopy of Rubidium D2 Transitions

Ebram Youssef* and Peter Brown†
Department of Physics, University of Rochester, Rochester, New York 14627, USA
(Dated: October 20, 2022)

Precise atomic spectroscopy is an important application of Laser physics and has great significance in numerous fields. In this study, saturated absorption of rubidium vapor was used as a Doppler-free spectroscopy technique in order to identify narrow spectral features and hyperfine structures in the Rubidium D2 line. A single grating-feedback diode laser was utilized in a pump-probe optical setup in order to observe and record both Doppler-broadened and Doppler-free spectra. Analysis of the two spectra shows a higher resolution of atomic transitions was reached by saturated absorption, as proposed. A comparison of measured and theoretical transition frequencies of hyperfine-split ground and excited states of Rubidium demonstrates relative agreement within the uncertainty limits of the measurements.

I. INTRODUCTION

Absorption spectroscopy is the measurement of how much light is absorbed by a specific matter (*i.e., atomic vapor, in this case*) over a set spectral range [1]. if the wavelength of the electromagnetic radiation corresponds to a photon energy that matches the energy difference between two levels in the atoms, a portion of the light will be absorbed and re-emitted by the atoms. This is known as the resonance condition [2]. Lines on the spectral range corresponding to the resonance condition at each transition are known as spectral lines. Identifying spectral line profiles with high precision and resolution has a multitude of significant applications, including better understanding atomic structures and transitions, metrology, sensing, frequency references for optical clocks, defining elemental composition, determining fundamental physics constants, precise measurement of the proton-electron mass ratio, exploring Quantum Electrodynamics (QED), and many more [3].

In this spectroscopy study, a vapor cell containing the two naturally occurring isotopes of rubidium, ^{85}Rb (72% abundance) and ^{87}Rb (28% abundance) was used. Due to the random motion and distribution of velocities of individual rubidium atoms inside the cell, a beam of coherent light with a specific wavelength and frequency moving in some direction through the cell will be perceived to have a longer wavelength (red shift) for atoms having a velocity component that is parallel to the beam's direction of propagation, a shorter wavelength (blue shift) for atoms with a velocity component anti-parallel to the beam's propagation, and a wavelength corresponding to the actual frequency of the light beam for atoms having no velocity component along the axis of the beam's propagation (*i.e., atoms strictly moving in a transverse direction with respect to the propagation of the light beam*). This effect is known as the Doppler shift. Fig. 1 shows a graphic demonstration of said effect.

When a frequency sweep is performed on the diode laser emitting this light beam, rubidium atoms inside the vapor cell that are moving with anti-parallel longitudinal velocities will see the light to have a higher frequency (and hence higher energy). If the resonance frequency is $\nu_\circ$, and the current frequency of the light beam is $\nu_\circ - \Delta\nu$, then the beam will only be absorbed by atoms moving with an anti-parallel (moving towards the beam) longitudinal velocity of $\approx \frac{c\cdot\Delta\nu}{\nu_\circ}$ [4]. These atoms perceive the beam to be blue-shifted into resonance, and hence get excited by it. The same effect is present throughout the frequency sweep for different values of $\Delta\nu$, and the opposite effect is true for atoms moving away from the beam, which perceive a light beam of frequency $\nu_\circ + \Delta\nu$ to be red-shifted into resonance. Therefore, the absorption spectrum in the presence of Doppler shifts is broadened around the resonance frequency. This is known as Doppler broadening. Due to the random

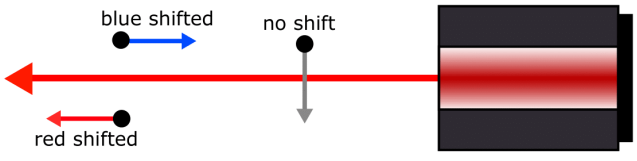

FIG. 1: A simple graphic demonstration of the Doppler effect.

* Main Author; eyousse2@u.rochester.edu
† Laboratory Partner

nature intrinsic to the motion of atoms in relatively high temperatures, the longitudinal velocity distribution of rubidium atoms follows a Maxwell-Boltzmann velocity distribution centered about zero, and hence the Doppler-broadened spectra exhibit a Gaussian-like profile around the resonant frequency. Fig. 2(a) shows the Maxwell-Boltzmann velocity distribution in the longitudinal direction for room temperature rubidium atoms. Fig. 2(b) shows a qualitative comparison of arbitrary broadened and unbroadened spectra [5].

In the case of rubidium vapor, the observed Doppler broadening is on the order of $\Delta\nu \sim 1\ GHz$. Which is much larger than the natural linewidth of the transition for rubidium D lines, $\Gamma = 6\ MHz$. This considerable increase in linewidth of the spectrum greatly decreases the resolution and precision of the spectral features, which is a necessity for all the aforementioned applications of spectroscopy. Saturated absorption spectroscopy is a simple and common technique for measuring narrow-line atomic spectral features, limited only by the natural linewidth Γ of the transition. The following section explains in detail the physics and theory of saturated absorption.

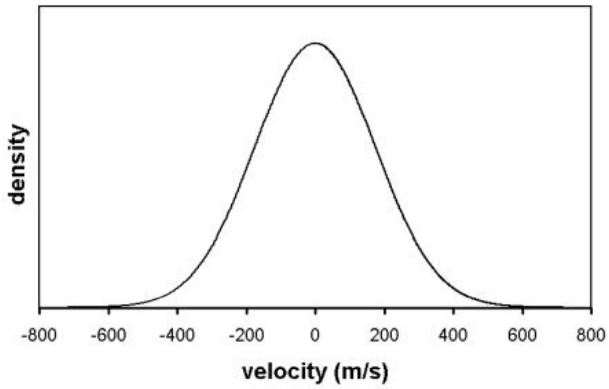

(a)

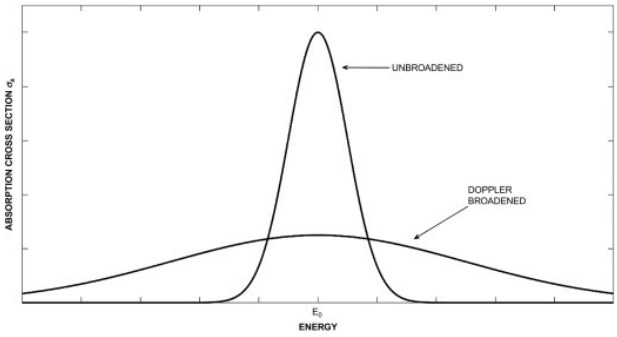

(b)

FIG. 2: (a) Arbitrary Maxwell-Boltzmann velocity distribution in the longitudinal direction for room temperature rubidium atoms. (b) Qualitative comparison of broadened and unbroadened spectra.

II. THEORY

A. Saturated absorption spectroscopy

Laser spectroscopy in atomic vapor in temperatures akin to room temperature is often limited by Doppler broadening. One popular technique to overcome the Doppler effect broadening is saturated absorption spectroscopy. In this method, a low-intensity probe and high-intensity pump beams are derived from the same source of some coherent frequency. The beams are then sent through the vapor cell in opposite direction such that the two beams are exactly collinear and counterpropagating (Fig. 3). Since the two beams have opposite propagation, they cause opposite Doppler shifts, and hence only the zero-velocity atoms (*i.e., those moving strictly orthogonally with respect to the beams' propagation directions*) interact with both beams [6].

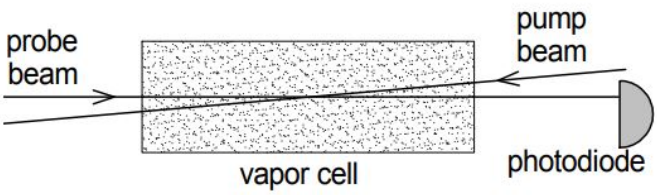

FIG. 3: Pump-probe counterpropagation inside the vapor cell. The beams must be collinear, but appear at an angle in this picture for demonstration purposes.

When the frequency scan reaches the resonance frequency ($\nu = \nu_\circ$), the zero-velocity atoms perceive both beams to be at resonance, but since the pump beam is much more intense than the probe, it saturates the zero-velocity atoms almost indefinitely. This, subsequently, causes there to be a peak of probe transmission at resonance, which produces a sharp, Doppler-free spike at the resonance. The linewidth of this Doppler-free spike is only limited by the natural linewidth of transition ($\Gamma = 6$ MHz for Rb D lines).

Due to the counterpropagation of the beams, the presence of the pump beam doesn't affect the probe transmission at frequencies other than resonance, since their Doppler shifts are opposite. Since the distribution of atom velocities in the vapor is approximately Maxwell-Boltzmann, the density of zero-velocity atoms is high enough for this Doppler-free spike to be well-defined on the absorption spectrum, given the collinearity and counterpropagation conditions are met. In theory, using this technique reduces the transition linewidth from a few Gigahertz to as little as 6 MHz, and hence considerably increasing the resolution of spectral features in atomic vapors.

Fig. 4(a) shows the effect of saturated absorption for a two-level atom, which is one that has one distinct ground state and one distinct excited state with separation greater than the Doppler width, and hence one distinct resonance frequency. However, most real atoms are multi-level atoms, where electromagnetic multipole interaction between the nucleus and electron orbits cause excitation states to split into multiple hyperfine levels, which is known as hyperfine splitting. This causes there to be multiple resonances, and hence multiple Doppler-free spikes on the absorption spectrum. These hyperfine states are very closely spaced (*i.e., separation much less than Doppler width*), which results in what's known as 'crossover' peaks or resonances.
These crossover resonances occur when the beam is tuned exactly halfway between two resonances, and so for some velocity population the pump drives one transition while the probe drives the other transition. By definition, these crossover peaks occur at [4]

$$\frac{\nu_1 + \nu_2}{2} \tag{1}$$

Fig. 4(b) shows the effect of saturated absorption on atoms with 2 hyperfine excitation states and a crossover resonance.

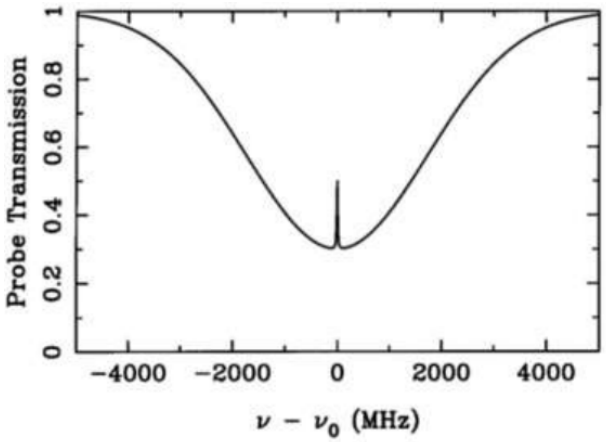

(a)

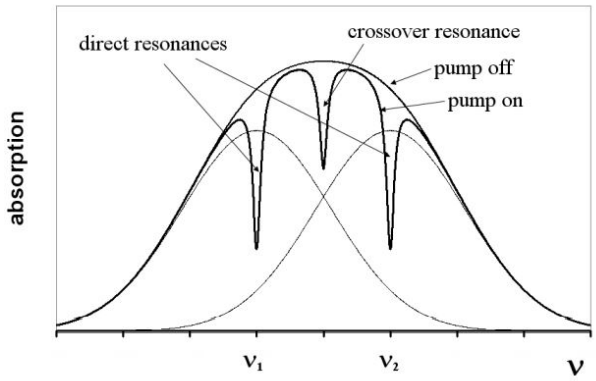

(b)

FIG. 4: Effect of saturated absorption on probe transmission for (a) a two-level atom and (b) a multilevel atom with 2 hyperfine excitation states and a crossover resonance.

B. Atomic Structure of Rubidium [7] [8]

Rubidium is an interesting element for a spectroscopy study due to its electronic configuration and atomic structure. At ground state, the electronic configuration of rubidium consists of closed shells and a single valence electron is the 5s orbital. For the first excited state, the single valence electron moves up to the 5p orbital (D transitions, $L = 0 \rightarrow L = 1$). In general, rubidium has a spin quantum number S of 1/2, due to the contribution of a single valence electron. More specifically, ^{85}Rb has a nuclear spin quantum number I of 5/2, and ^{87}Rb has $I = 3/2$. The fine structure is a result of the coupling between the orbital angular momentum L of the outer electron and its spin angular momentum S. The total electron angular momentum is then given by $J = L + S$. The corresponding quantum number J must, therefore, lie in the range $|L - S| \leq J \leq L + S$.
For the ground state, $S = 1/2$, $L = 0$ (for S orbitals), and $J = 1/2$. Hence, the ground state of rubidium is $5\,^{2S+1}S_J = 5\,^2S_{1/2}$.
For the excited state, $S = 1/2$, $L = 1$ (for P orbitals), giving either $L = 1/2$ or $L = 3/2$, which gives off two excitation states, $5\,^2P_{1/2}$ and $5\,^2P_{3/2}$. The first of the two is associated with D1 transitions, and the latter with D2 transitions. Only D2 transitions ($5\,^2S_{1/2}$ to $5\,^2P_{3/2}$) were considered in this study. The transition frequency of rubidium D2 line is $\omega_\circ = 2 \cdot \pi \cdot 384.23\ THz$, with an isotope shift of $\omega_\circ(^{87}\text{Rb}) - \omega_\circ(^{85}\text{Rb}) = 2 \cdot \pi \cdot 78.1\ MHz$.
Spin-orbit coupling interactions lead to magnetic hyperfine splitting of energy levels. More specifically, the hyperfine structure is caused by the coupling of J with the total nuclear angular momentum I. The total atomic angular momentum F is then given by $F = J + I$. Therefore, the magnitude of F must lie in the range $|J - I| \leq F \leq J + I$.
For the ground state $5\,^2S_{1/2}$ of ^{85}Rb, $J = 1/2$, $I = 5/2$, and so $F = 2$ or $F = 3$ (two hyperfine split ground states). For the D2-line excited state $5\,^2P_{3/2}$, F could be $= 1, 2, 3, or\ 4$ (four hyperfine split excited state). For the ground state of ^{87}Rb, $J = 1/2$, $I = 3/2$, and so $F = 1$ *or* 2. For the D2-line excited state, $F = 0, 1, 2, or\ 3$. The hyperfine splitting for energy levels of $J = 1/2$ (the case studied here) is simply given by the Hamiltonian

$$H_{hfs} = A_{hfs} \boldsymbol{I} \cdot \boldsymbol{J} \tag{2}$$

Where A_{hfs} is the magnetic dipole hyperfine structure constant for each isotope of rubidium. This Hamiltonian

leads to a hyperfine energy shift of

$$\Delta E_{hfs} = \frac{1}{2} A_{hfs}[F(F+1) - I(I+1) - J(J+1)] \quad (3)$$

Tables I and II summarize all the constants associated with ^{85}Rb and ^{87}Rb D2 transitions that were needed for calculating the theoretical values of transition energies and hyperfine energy shifts used in this study based on the relations given above. Fig. 5(a) shows the hyperfine energy level diagrams for ^{85}Rb and ^{87}Rb D2 transitions. Fig. 5(b) shows the typical absorption spectrum for a rubidium vapor cell consisting of 85 Rb and 87 Rb, with thermal Doppler broadening in effect. More in-depth information on the D line data of 85 Rb and 87 Rb could be found in a study conducted by Daniel Steck (ref. 7 and 8). All aforementioned information and data in this subsection were based on these two references.

III. EXPERIMENT

A. Setup

A complete schematic of the optical setup used is given in Fig 6. A TeachSpin grating-stabilized diode laser was placed at one end of the optical table. The laser is both temperature- and current-regulated. The laser temperature was set to $\sim 24°C$. Both the horizontal and vertical gratings were aligned for optimal Rb fluorescence. The laser current was set according to the value listed in the manufacturer's data sheet for optimal fluorescence, which did correspond to the most refined fluorescence lines in this setup as well. The laser is controlled such that it performs a frequency scan of relatively large size ($\sim 20GHz$) around the frequency corresponding to the set current and temperature. A single coherent laser beam then enters an ND glass filter, which operates as an optical isolator to prevent external feedback reflecting back to the laser. The beam then propagates through a 1° wedged 10/90 beam splitter. The splitter outputs three beams. On one side, an intense beam is produced, which is used as the pump beam in this experiment. On the other side, two equally weak beams are produced with a slight angle shift in their propagation directions. One of them serves as a probe beam, and the other serves as a 'reference' beam, which is used for background subtraction of the spectrum. Both the probe and reference beams propagate further to the Rb vapor cell. The thermal control of the vapor cell's heater was set to $50.0 \pm 0.2°C$, which corresponds to a vapor density that exhibits a strong absorption signal. The optimal temperature for absorption is $45°C$, as per the manufacturer's data sheet. However, a cell temperature of $50.0°C$ still produces a noticeable (about 90%) absorption signal. After propagating through the cell assembly, the probe beam goes through a 50/50 beam splitter, and then hits photodetector (PD) 1. The reference beam goes directly towards photodetector 2. The pump beam is then split using a cube beam splitter into two beams, one, using the help of a set of mirrors, propagates back towards the vapor cell such that it is completely collinear and counterpropagating with respect to the probe beam, which is the basis of saturated absorption. The other beam propagates through a Fabry-Pérot cavity, which is used for frequency calibration. The beam exiting the FP cavity then lands on photodetector 3. A CCD camera setup is set next to the cell assembly, which is used for observing the fluorescence lines of rubidium inside the vapor cell.

B. Procedure

Initially, the pump beam is blocked, using a card or a piece of paper, such that it doesn't reach the Rb cell. This is done in order to observe the Doppler-broadened absorption spectrum similar to that shown in Fig. 5(b). The transmission of the probe beam is recorded via photodetector 1 and displayed on a Tektronix TDS 2002B oscilloscope. Then, the pump beam is allowed to propagate through the cell, and the transmission of the probe beam is once again recorded and displayed. This time, the resulting spectrum is that of a Doppler-free saturated absorption. The transmission signal of the reference beam, which is unaffected by the pump and hence shows a broadened spectrum, is recorded via photodetector 2. The signal from PD 1 and PD 2 are mathematically subtracted with different weight coefficients (balances) in order to remove the Doppler-broadened background and end up with only the Doppler-free spectrum. Different balances are used

TABLE I: Constants associated with ^{85}Rb D2 transitions and hyperfine splittings

Frequency	$\omega_\circ$	$2\pi \cdot 384.23\ THz$
Transition Energy	$\hbar\omega_\circ$	$1.589eV$
Wavelength (Vacuum)	λ	$780.24\ nm$
Wavelength (Air)	λ_{air}	$780.03\ nm$
Natural Linewidth (FWHM)	Γ	$2\pi \cdot 6.07\ MHz$
Magnetic Dipole Constant, $5^2S_{1/2}$	$A_{5^2S_{1/2}}$	$h\ \cdot 1.01\ GHz$
Magnetic Dipole Constant, $5^2P_{3/2}$	$A_{5^2P_{3/2}}$	$h\ \cdot 25.00\ MHz$

TABLE II: Constants associated with ^{87}Rb D2 transitions and hyperfine splittings

Frequency	$\omega_\circ$	$2\pi \cdot 384.23\ THz$
Transition Energy	$\hbar\omega_\circ$	$1.589eV$
Wavelength (Vacuum)	λ	$780.24\ nm$
Wavelength (Air)	λ_{air}	$780.03\ nm$
Natural Linewidth (FWHM)	Γ	$2\pi \cdot 6.07\ MHz$
Magnetic Dipole Constant, $5^2S_{1/2}$	$A_{5^2S_{1/2}}$	$h\ \cdot 3.42\ GHz$
Magnetic Dipole Constant, $5^2P_{3/2}$	$A_{5^2P_{3/2}}$	$h\ \cdot 84.72\ MHz$

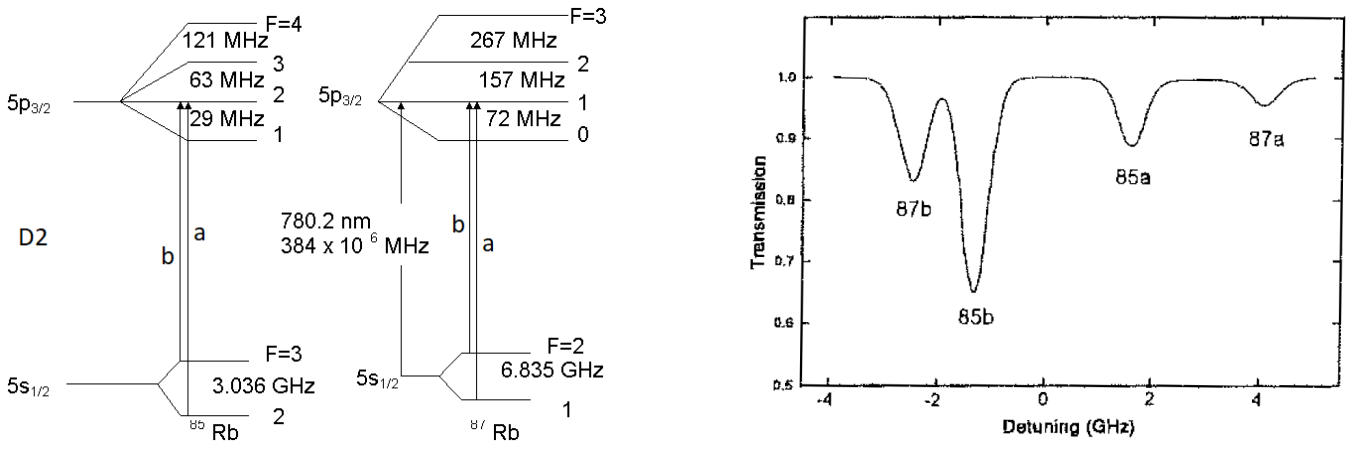

(a) (b)

FIG. 5: (a) Hyperfine energy level diagrams for ^{85}Rb and ^{87}Rb D2 transitions. (b) Typical absorption spectrum for a rubidium vapor cell consisting of 85 Rb and 87 Rb, with thermal Doppler broadening in effect.

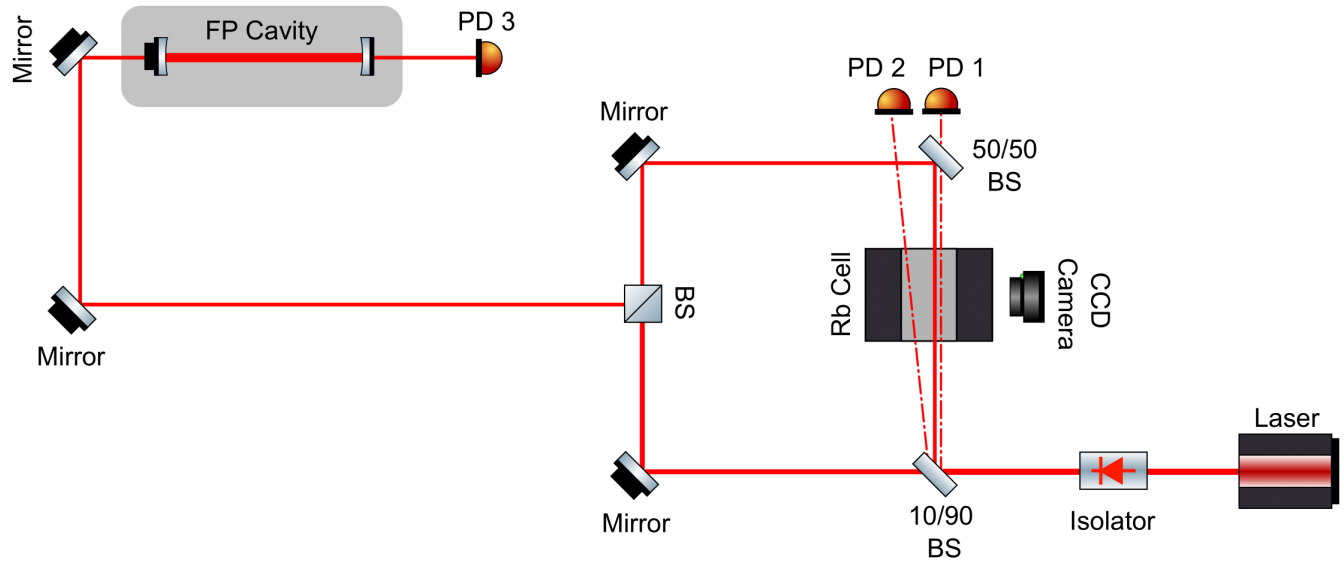

FIG. 6: Complete schematic of optical setup used for the purposes of this experiment.

in the subtraction for two reasons: (1) the reference beam, unlike the probe beam, doesn't propagate through the 50/50 splitter, and hence has a higher intensity, and (2) the photodetectors aren't always perfectly aligned with the beams, so one might pick up more signal than the other. The balance values are varied until good subtraction with little noise is reached. The subtraction is never perfect, which is caused by the two aforementioned reasons, and there will always be some residual background noise in the subtracted data, but it should be minimized – without significant loss of data – within the limitations of the setup.

The resonance transmission signal of the FP cavity is recorded via PD 3 and is displayed on the oscilloscope along with the absorption spectrum. The transmission peaks serve as 'markers on a ruler', which then defines the frequency range of the concurrent absorption spectrum. In order for these markers, and hence the whole spectrum, to have minimal uncertainty, the beam going through the cavity needs to be aligned exactly through the centers of both cavity mirrors, which allows for only one resonance mode to be transmitted through the cavity. The cavity length, which primarily impacts the spacing between adjacent peaks as explained in detail in the analysis section, also affects the width, and hence the uncertainty, of the markers.

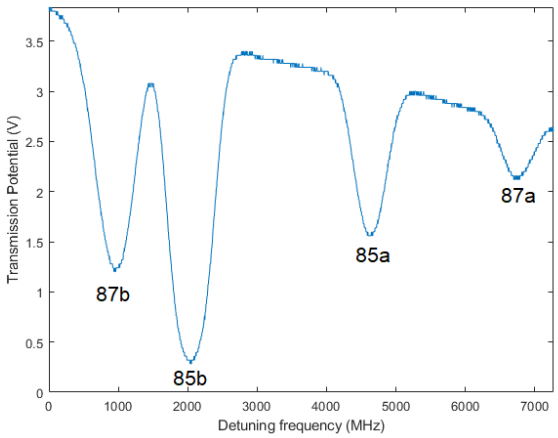

(a)

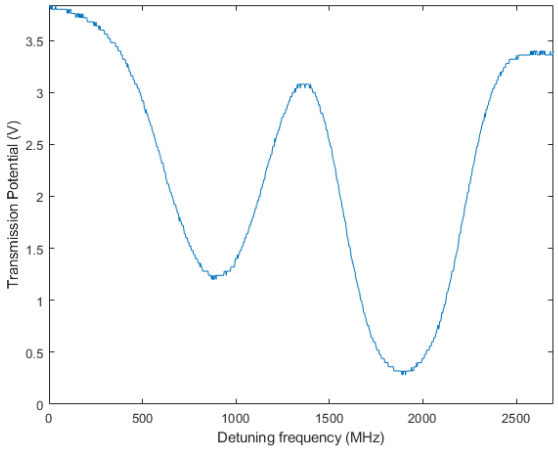

(b)

FIG. 7: (a) Full Doppler-broadened absorption spectrum showing, from left to right, 87b ($5^2S_{1/2}$, $F = 2$ to $5^2P_{3/2}$ for ^{87}Rb), 85b ($5^2S_{1/2}$, $F = 3$ to $5^2P_{3/2}$ for ^{85}Rb), 85a ($5^2S_{1/2}$, $F = 2$ to $5^2P_{3/2}$ for ^{85}Rb), and 87a ($5^2S_{1/2}$, $F = 1$ to $5^2P_{3/2}$ for ^{87}Rb) absorptions. (b) Doppler-broadened spectrum zoomed-in on 87b and 85b absorptions.

IV. RESULTS

For all of the spectra shown in this section, the x-axes represent the relative frequency (or frequency detuning) in units of MHz, rather than an absolute one. The absolute frequency of spectral features isn't of significance for the scope of this study, and only the transitions' separation frequencies are studied and analyzed. The y-axes represent probe transmission recorded by the photodetectors in units of volts. The absolute transmission values are also irrelevant to this study and were chosen to be represented in relative potential differences as recorded by the photodetectors.

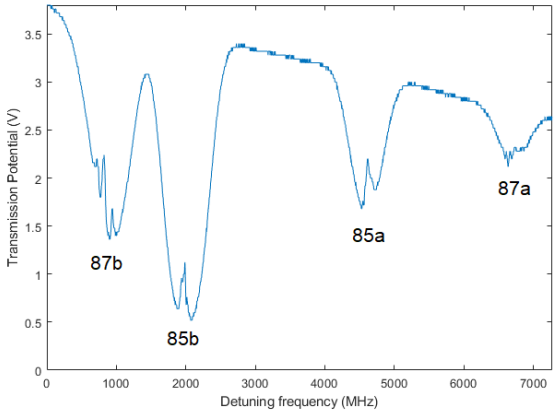

(a)

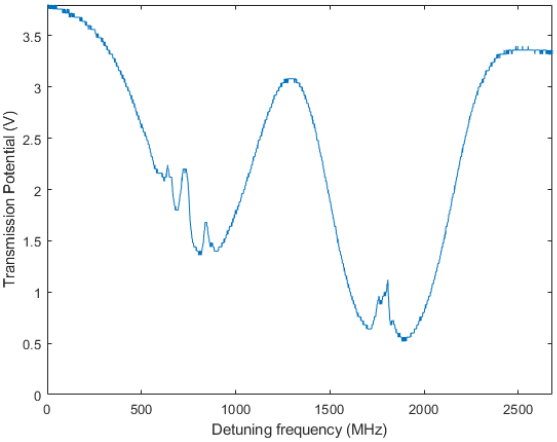

(b)

FIG. 8: (a) Full Doppler-free saturated absorption spectrum showing, from left to right, 87b, 85b, 85a, and 87a absorptions. (b) Doppler-free saturated absorption spectrum zoomed-in on 87b and 85b absorptions.

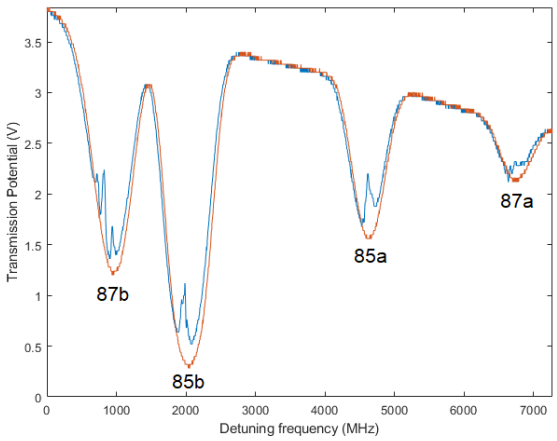

FIG. 9: Superimposition of full Doppler-broadened and Doppler-free spectra.

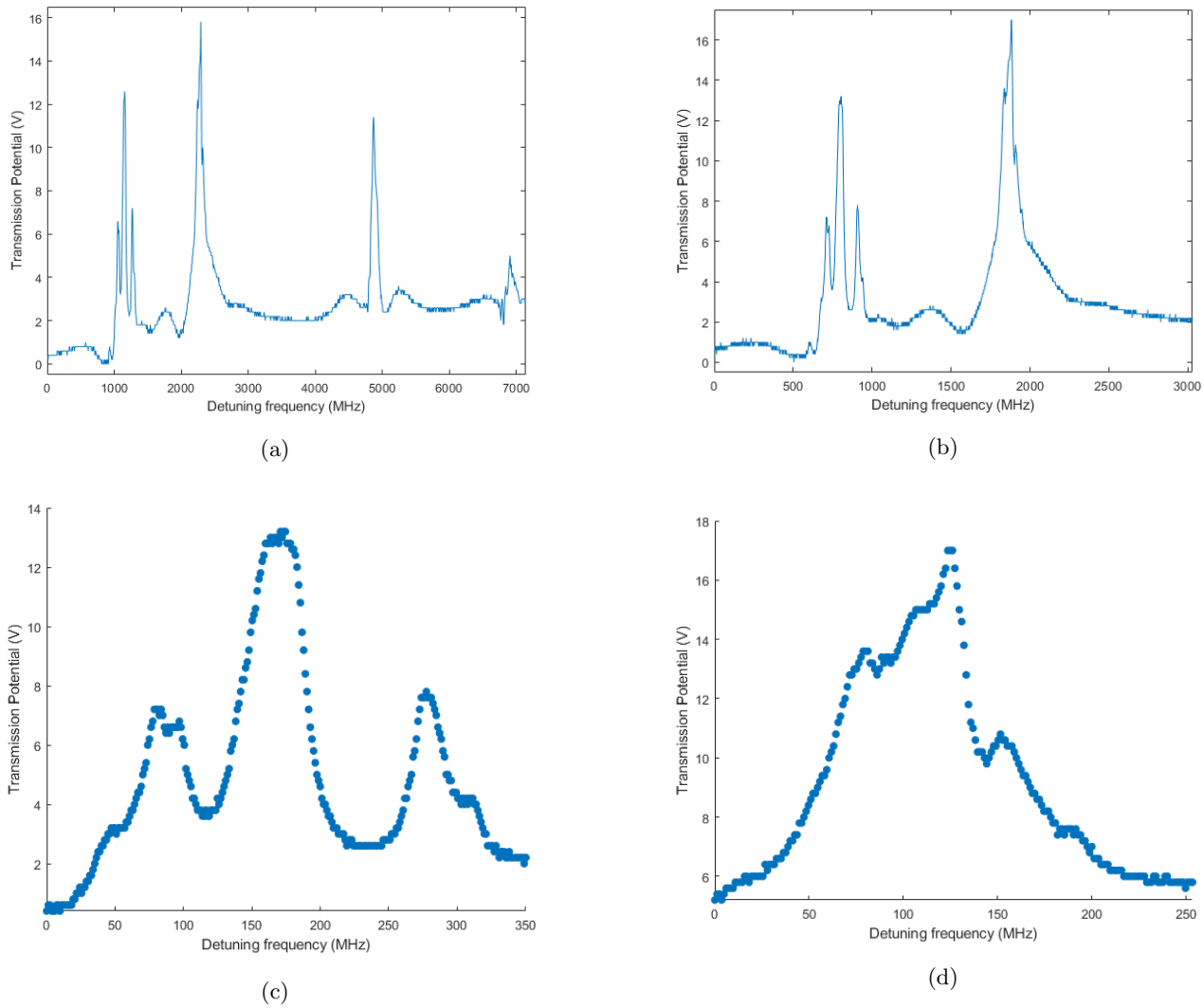

FIG. 10: (a) Full Doppler-free saturated absorption spectrum with Doppler background subtracted, showing some hyperfine and crossover transitions. (b) Background-subtracted absorption spectrum zoomed-in on 87b and 85b absorptions. (c) Background-subtracted data zoomed-in on 87b. (d) Background-subtracted data zoomed-in on 85b.

V. ANALYSIS

a. Fabry-Pérot frequency calibration The difference between adjacent maxima for FP resonance is defined as the free spectral range (FSR). For the 'bow-tie' mode patterns that are observed in the FP resonance for this experiment, the free spectral range is

$$FSR = \frac{c}{4L} \tag{4}$$

Where c is the speed of light and L is the length of the cavity. The length of the cavity was measured multiple times by a ruler, and the readings were recorded. The length of the cavity was found to be 23.07 ± 0.16 cm. This corresponds to an FSR of 324.89 ± 2.3 MHz. Fig. 12(a) shows the raw resonance signal captured by photodetector 3. The multiple modes in each peak are caused by suboptimal beam alignment within the cavity, which also causes the overall peaks to be relatively wide. A smoothing-spline fit was performed on this signal via MATLAB in order to refine each peak to a single mode, which makes it systematically easier to find peaks, their differences, and their widths. Fig. 12(b) shows the FP resonance after fitting. The difference between adjacent peaks in milliseconds is $\Delta t = 1.07 \pm 0.02$ ms. The conversion factor from time scale to frequency scale is $FSR/\Delta t = 302.8 \pm 2.15$ MHz. The average full width at half-maximum (FWHM) of the FP resonance peaks was 84.6 MHz, which corresponds to a peak standard deviation of $FWHM/2\sqrt{2\ln 2} \approx FWHM/2.355 = 35.92$ MHz. This leads to a total error in the frequency calibration of $\sigma_f = 38.07$ MHz. As could be noticed in Fig. 12(b), the finesse of the cavity (defined as

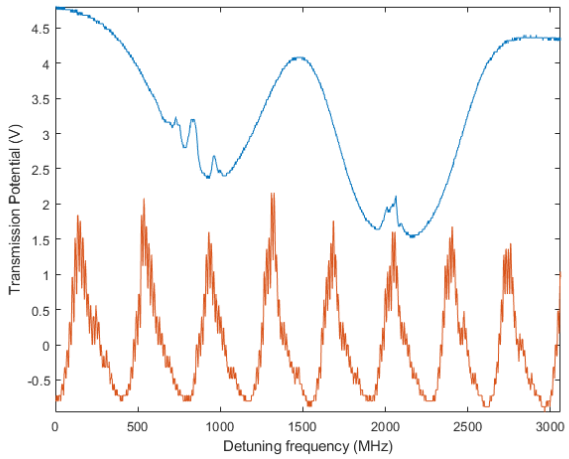

FIG. 11: Sample of FP calibration.

FSR/FWHM) is quite low (≈ 3.85). This greatly increases the uncertainty in frequency calibration. Better alignment of the beam onto the cavity mirrors, typically one that leads to a resonance signal of finesse greater than 100, would result in significantly better accuracy in frequency calibration. Additionally, using a more accurate method of finding FSR, such as using sidebands in the laser frequency sweeps, would further increase the accuracy of this operation.

b. Hyperfine transitions, theory vs results Fig. 13(a) and 13(b) show smooth fits of 10(c) and 10(d), respectively. Vertical lines are the positions of suspected hyperfine transitions (black) and crossover transitions (red). The measured transition frequencies of the 85b and 87b lines are compared with their theoretical counterparts calculated in the theory section in Tables III and IV, respectively. Additional uncertainty is added to that of the frequency scale due to the width of each hyperfine transition peak. The overall uncertainty of each transition was calculated by $\sqrt{\sigma_f^2 + \sigma_w^2}$, where σ_w is the sum of peak standard deviations of the two hyperfine transition peaks in consideration for each transition peak separation calculation. The measured values generally seem to agree with the theoretical ones within the uncertainty limits. The uncertainty values in transition measurements were quite large, which could be attributed to multiple reasons, including suboptimal cavity-beam alignment, suboptimal pump-probe alignment, fuzziness and noise in the electronic components used for measurements (i.e., photodetectors, oscilloscope, etc.), imperfect background subtraction, and suboptimal vapor cell temperature, which should be set at $45°C$, rather than $50°C$. The improper cell temperature was specifically significant to the results, since Doppler broadening is based on thermal effects, and so the saturated absorption spectrum was less refined as it might be at optimal temperature.

c. Resolution of absorption peaks, Doppler-broadened vs Doppler-free The FWHM of absorption peaks is an

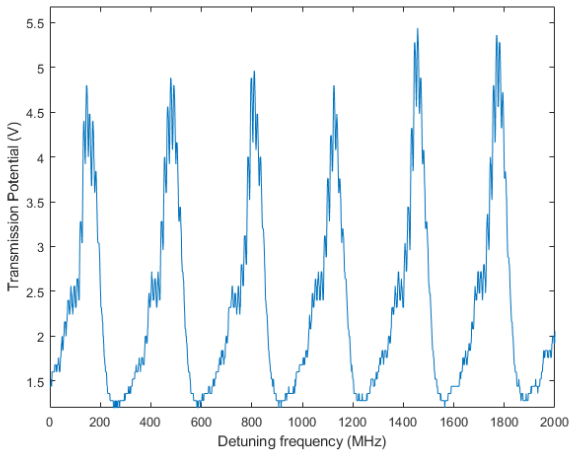

(a)

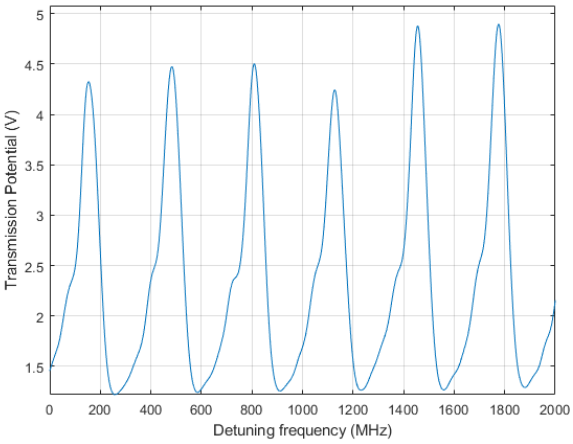

(b)

FIG. 12: (a) Raw FP resonance signal. (b) FP resonance with an applied smoothing fit.

TABLE III: Measured vs. theoretical peak separation of 85b transitions

Transition	Measured (MHz)	Theoretical (MHz)
F = 1, F = 2	10.91 ± 42.18	29
F = 2, F = 3	33.93 ± 42.82	63
F = 3, F = 4	65.43 ± 45.39	121

TABLE IV: Measured vs. theoretical peak separation of 87b transitions

Transition	Measured (MHz)	Theoretical (MHz)
F = 0, F = 1	48.46 ± 41.68	72
F = 1, F = 2	72.70 ± 58.30	157
F = 2, F = 3	141.00 ± 57.78	267

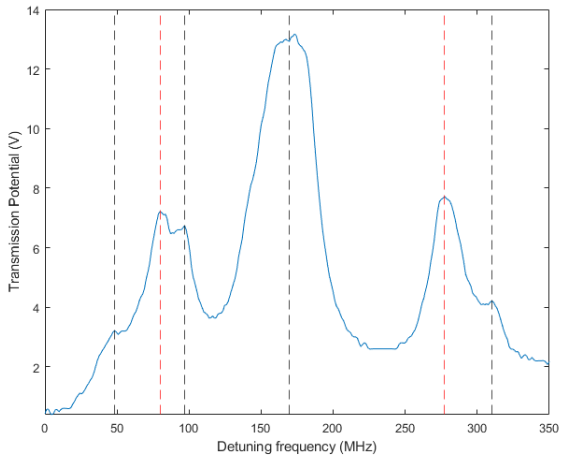

(a)

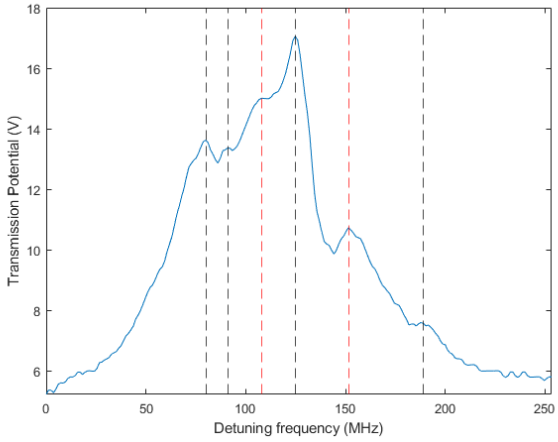

(b)

FIG. 13: (a) 87b spectrum smooth fit with suspected peaks marked. (b) 85b spectrum smooth fit with suspected peaks marked.

important indicator of the accuracy and resolution of any spectroscopy. The FWHM of the measured Doppler-broadened 87b absorption was found to be 510.46 MHz, while the average FWHM of the Doppler-free hyperfine absorption peaks identified above was 14.33 MHz. This results in a FWHM reduction of 97.19%. The FWHM of Doppler-broadened 85b absorption was 607.68 MHz, while the average FWHM of the Doppler-free absorption peaks was 6.74 MHz, which results in a FWHM reduction of 98.89%. These reduction percentages are an indicator for the high efficiency of saturated absorption as a Doppler-free spectroscopy technique. Additionally, the linewidth of the Doppler-free absorption peaks was comparable to that of the natural linewidth of rubidium (Gamma = 6 MHz), which intrinsically defines the lower limit of peak width, unlike the Doppler-broadened peaks which were about 3 orders of magnitude greater.

VI. CONCLUSIONS

Saturated absorption as a method of reducing thermal Doppler broadening was shown to be effective to great extents. Ultimately, the results of this spectroscopy technique may affect a variety of important applications dependent on these narrow transitions, including optical clocks, quantum information, determination of fundamental constants, and investigating physics beyond the standard model. Hyperfine transitions in Doppler-free absorption spectra were identified, and the measured separation frequencies of transitions mostly agreed with those predicted by theory, within the uncertainty limits. Uncertainty values, and consequently accuracy of spectroscopy, could be reduced if the aforementioned sources of errors are treated. For future studies, it is recommended that the FP cavity mirrors has better alignment with the laser beam, such that higher finesse levels are reached. Additionally, a lower cell temperature should be maintained for optimal vapor density. More involved optical techniques could be followed to maintain better pump-probe, as well as beam-cavity, alignment, and hence more refined saturated absorption spectra.

ACKNOWLEDGMENTS

The author would like to thank Professor Nick Bigelow, Mike Culver, and Kagan Yanik for their continuous help throughout this study, as well as Peter Brown, the author's laboratory partner. The author acknowledges the usage of a vector graphics library by gwoptics to create schematics used in this article. Other figures in this manuscript were based on, or directly taken from, other sources as well.

[1] C. N. Stedwell and N. C. Polfer, Laser photodissociation and spectroscopy of mass-separated biomolecular ions, Lecture Notes in Chemistry 10.1007/978-3-319-01252-0 (2013).

[2] A. Sanz-Medel, J. Costa, and R. Pereiro, Atomic spectrometry, in *Reference Module in Chemistry, Molecular Sciences and Chemical Engineering* (Elsevier, 2013).

[3] Y.-N. Lv, A.-W. Liu, Y. Tan, C.-L. Hu, T.-P. Hua, X.-B. Zou, Y. R. Sun, C.-L. Zou, G.-C. Guo, and S.-M. Hu,

Fano-like resonance due to interference with distant transitions, Phys. Rev. Lett. **129**, 163201 (2022).
[4] Diode laser spectroscopy student manual (TeachSpin, Inc).
[5] T. KERLIN, *Dynamics and control of nuclear reactors* (ELSEVIER ACADEMIC PRESS, 2020).
[6] A. Banerjee and V. Natarajan, Saturated-absorption spectroscopy: eliminating crossover resonances by use of copropagating beams, Opt. Lett. **28**, 1912 (2003).
[7] D. A. Steck, Rubidium 85 d line data, (2021).
[8] D. A. Steck, Rubidium 87 d line data, (2021).